

Effect of Sampling Orientation on The Mechanical Properties of Glass Fiber Reinforced Epoxy Nanocomposites

Gökhan Demircan^{1*} 

^{1*} Harran University, Faculty of Engineering, Department of Mechanical Engineering, Şanlıurfa, Türkiye,
gdemircan@harran.edu.tr

*Corresponding Author

ARTICLE INFO

Keywords:
Glass Fiber
Polymer
Nanocomposite
Mechanical Properties
Sampling Orientation

Article History:

Received: 16.09.2023

Accepted: 08.11.2023

Online Available: 27.02.2024

ABSTRACT

Fiber-reinforced polymer composites are manufactured using various methods, with vacuum-assisted resin transfer molding (VARTM or VARIM). This study's primary focus lies in assessing how the orientation of sampling impacts the mechanical properties of glass fiber-reinforced pure and nanocomposites. 2 wt.% nano Al₂O₃-doped and non-doped composites were produced using the VARTM process. Tensile, flexural, and density test specimens were extracted from three distinct zones and two distinct directions those aligned horizontally to the resin flow (HRF) and those oriented vertically to the resin flow (VRF). Remarkably, results showed up to a 3.91% increase in values from samples in the third zone, particularly on the vacuum outlet side. To facilitate precise stress value comparisons across plates, uniform sample orientation and consistent zone selection are essential.

1. Introduction

Composite materials have brought a new age in materials engineering science, allowing engineers to create superior materials with outstanding mechanical characteristics. Fiber-reinforced polymer composites (FRP) are one of them and are made up of two major components: a load-bearing component, such as fibers, and a polymer medium that acts as a binding and protection for the fibers [1-3]. The polymer matrix plays a pivotal role in ensuring the fibers maintain their orientation and structural integrity, while also facilitating the transfer of loads. Typically, thermoset or thermoplastic materials are chosen for the polymer matrix [4, 5]. Meanwhile, the fibers primarily shoulder the load transmitted from the matrix, imparting macroscopic stiffness and strength to the structure. Commonly used reinforcing fibers include glass, aramid, and carbon fibers. Such FRP composites are gaining prominence due to their exceptional resistance to corrosion,

impressive thermo-mechanical characteristics, and high strength-to-weight ratio [6, 7]. Their diverse range of properties makes them indispensable in a wide array of industries, including aerospace, marine, construction, biomedical, automotive, and many others [8-10].

The performance of composite materials is predominantly influenced by the quality of their constituent elements and the precision of their manufacturing processes. The manufacturing processes need to be investigated to determine the material's optimal properties for the specific purpose. Various approaches are viable, depending on the chosen reinforcement category and the intended product application [11, 12]. Some of them are as follows; hand layup [13], compression molding [14], filament winding [15], pultrusion [16], spray-up [17], resin transfer molding (RTM) [18], vacuum-assisted resin infusion method (VARIM) [19]. Since the 1950s, vacuum-assisted resin infusion method (VARIM) has been utilized to create fiber

reinforced polymer composites in different shapes [20-23]. This method is also referred to as vacuum assisted resin transfer molding (VARTM) in the literature [24]. The technique is a closed mold method for producing high-performance and large-scale fiber reinforced polymer (FRP) products with minimal tooling costs. Although large and complex composite parts can be produced in high quality with this method, there are some disadvantages. The possibility of air leakage is considerable, and this is highly dependent on the worker's ability, training, and the consumables (peel ply, vacuum bag, distribution medium etc.) condition of each VARIM operation. Dry spots and inadequate resin infusion might result from air leakage and can ruin the composite production [25]. Factors such as mold filling, fiber compaction, dry spot and micro-voids are the related processing issues to be considered in order to produce a stable composite.

The VARIM technique is also a key method in the production of nanoparticle enhanced FRP composites [26-28]. To create nanocomposite, nano-enhanced polymers can be injected into fiber mats composed of fibers such as carbon, aramid or glass fibers. Due to its unique through-thickness flowing profile the VARIM process has been recognized as a potential approach for producing nano-enhanced FRP among several production methods. However, through-thickness flow may not reduce the traveling distance of the nano resin flow along the fiber preform to the desired level [29]. As a result, the possibility of nanoparticles being filtered by the fiber preform increases. This nanoparticle filtration affects the distribution of nano-enhanced polymer blend in composite. This imperfection can also affect the mechanical properties of the nanocomposite. The porosity of the fiber preform also has an impact on nanoparticle filtering. Fan et al. [30] developed a new injection and double vacuum assisted resin transfer molding (IDVARTM) technique to decrease the impacts of porosity. The infusion is assisted by capillary pressure in this approach. This provided a high void formation, allowing the nano-doped resin to pass through the fiber with less nanoparticle filtration. Another VARTM-based technique to incorporating carbon nanofibers (CNFs) into FRP was

investigated by Movva et al. [31]. They used a solvent guided spray method to pre-bond the CNFs to the glass fiber matting. This technique may lower the risk of CNF filtering during resin infusion.

The literature review revealed that the VARTM or VARIM method was improved with different modifications to minimize nanoparticle filtration for nanocomposite production. However, the mechanical stability of the sample extraction zones of the nanocomposite plate produced by the traditional VARTM method is an important issue that needs to be investigated in detail. In this study, nano alumina (Al_2O_3) reinforced epoxy composites were produced by VARIM. Samples were taken from the composites in the directions horizontal to the resin flow (HRF) and vertical to the resin flow (VRF), and the mechanical properties of these directions were determined by tensile, three point bending and density tests. Also, ANOVA analysis was performed to determine the significance of the variables and to see if each variable has or not significant effect on tensile and flexural strength values.

2. Experimental Procedure

2.1. Materials

The nanoparticle to be used for nano reinforcement was aluminum oxide (Al_2O_3) with 78 nm average particle size (Nanografi). The purity of nanoparticles is 99.55%. MGS L285 epoxy resin and H287 hardener were used for obtaining nano-enhanced polymer (HEXION). It was chosen because it has a low viscosity (600-900 mPas). The resin-to-hardener ratio is 100:40 by weight. Plain weave-type glass fiber with an area weight of 200 gr/m² was used as the fiber reinforcement. A table type circular saw bench with water cooling system was used to cut the samples.

2.2. Production of glass fiber reinforced epoxy nanocomposite

Two different composites were produced by using the conventional VARTM method. One plate was produced in pure form and the other was produced using nano Al_2O_3 particles to study

the dispersion of the nanoparticle in polymer resin. The representation of the method is shown in Fig 1.

The following steps were applied for production.

- Release film was applied to prevent the composite plate from sticking to the bench.
- 16 layers of glass fiber were laid on the release film.
- A peel ply was applied for easy removal of the composite plate.
- Infusion mesh was applied on the top of the peel ply.
- A Spiral hose was used to provide a fast resin supply in the resin injection line.

- Ventilation ports are placed in the resin inlet and outlet region.
- The assembly was surrounded with sealing tape, which is a double-sided sticky adhesive.
- The vacuum bag was carefully laid on the assembly.
- Resin injection port was closed, and vacuum port opened to apply the vacuum.
- Pure resin and nano-enhanced resin were infused into the resin reservoir.
- After the vacuum port was closed, the system was left to cure at 80 °C for 15 h (bench heater) as mentioned by resin manufacturer.
- Demolding the composite part from the bench was successfully made. Fig. 2 shows a cured composite plate on the bench.

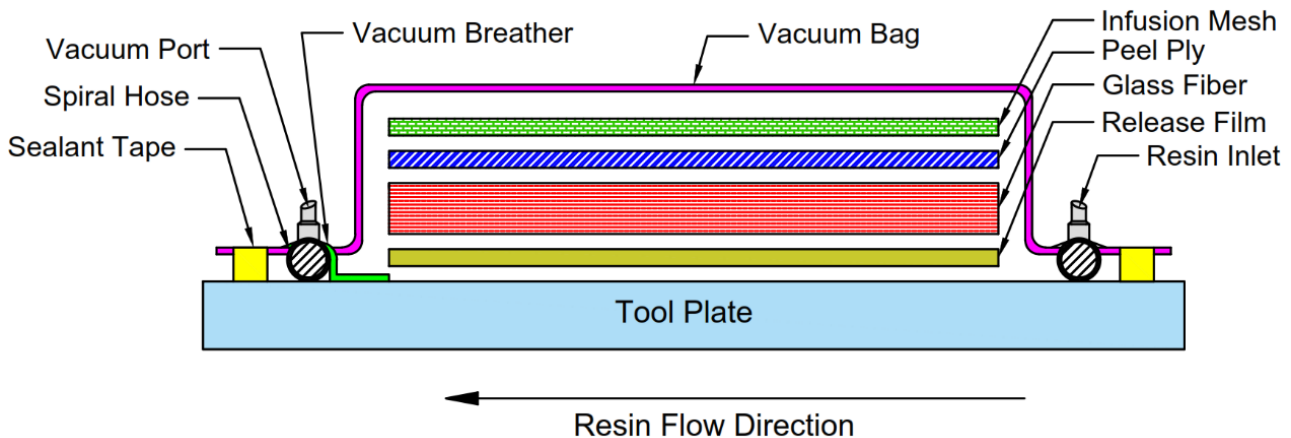


Figure 1. Schematic representation of VARTM

2 wt.% of Al₂O₃ nanoparticles was used to form nano-enhanced epoxy resin using the ultrasonic dual mixing method (UMM) [32]. Ultrasonic dual mixing is the employment of ultrasonic vibration and mechanical stirring at the same

time to shear the resin matrix. It has the ability to modify resin matrix and provide a homogeneous distribution of nanoparticles that is nearly cluster-free.

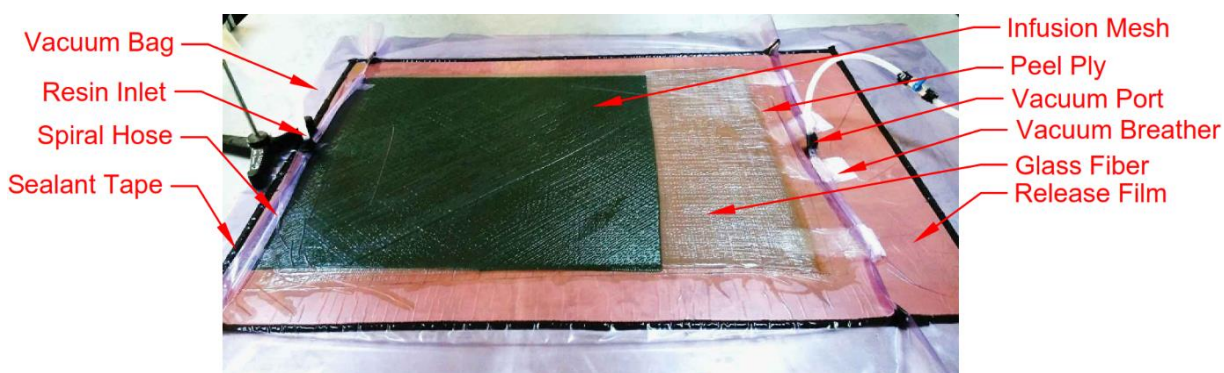


Figure 2. Cured composite plate on the bench

This was important in significantly improving the mechanical and physical characteristics of the polymeric basis composites. The ultrasonic

mixing was done with an ultrasonic stirrer (VCX 500, Sonics, USA) with a maximum power output of 750 W and a steady frequency of 20

kHz and a 50 mm diameter titanium alloy tip. A pulse of 2 s on and 3 s off was used to apply sonication with a 70% amplitude for 2 h. During sonication process a magnetic mixer (MR Hei-Tech, Heidolph, Germany) was used simultaneously at 400 rpm [5, 19, 26]. To achieve a successful dispersion, precautions were taken during UMM to ensure that the temperature of the polymer mixture did not rise throughout the mixing time. The mixing was done in a bowl bordered by an ice bath, and the temperature of the bath is tracked by immersing a temperature probe connected to the ultrasonic mixer to prevent an extreme increase in temperature during mixing. The schematic representation of UMM method is shown in Fig 3. Finally, two composite plates were produced for comparison purposes. One is pure plate without nanoparticle additive, and the other is nanoparticle doped plate.

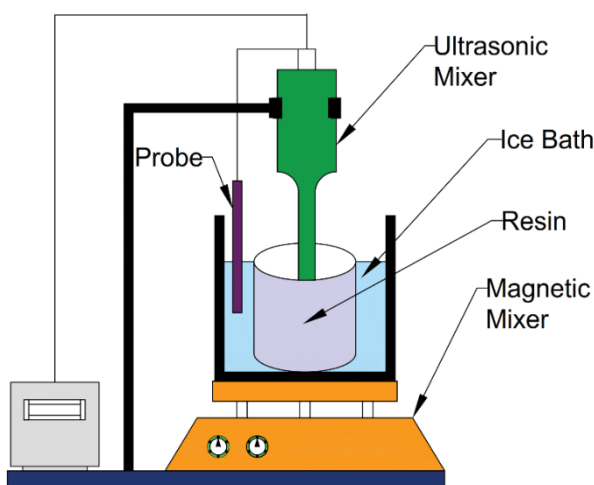


Figure 3. Schematic representation of UMM method

2.3. Mechanical tests and sampling orientation

Tensile and bending tests were performed in accordance with ASTM D3039/D3039M-17 [33] and ASTM D790-17 [34] using a Shimadzu AGS-X Plus Universal test machine. Density Measurement was carried out with Archimedes' principle with samples having $15 \times 15 \times 3.2 \text{ mm}^3$ dimensions. The bending test specimen's dimensions were determined to be $127 \times 12.7 \times 3.2 \text{ mm}^3$ and the dimensions of tensile test specimen were $250 \times 25 \times 3.2 \text{ mm}^3$. The strain rate was 2

mm/min for tensile test and 1 mm/min for bending test. Samples and dimensions were shown in Fig. 4.

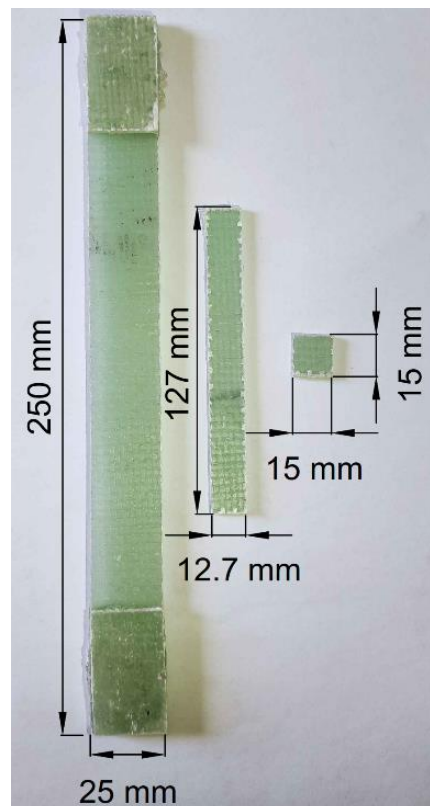


Figure 4. Test samples and dimensions

Two different plates were produced to examine the effect of nanoparticle filtration on the mechanical properties of the composite. One plate has no nanoparticles, while the other has 2 wt.% of nanoparticles. The plates were divided into 3 different zones to determine in which zones the filtration is effective along the vacuum line. In addition, to examine the effect of sample extraction directions, samples were extracted both vertical to the resin flow (VRF) and horizontal to the resin flow (HRF). Sample notations are given in Fig. 5. Sample extraction zones and orientations are shown in Fig. 6.

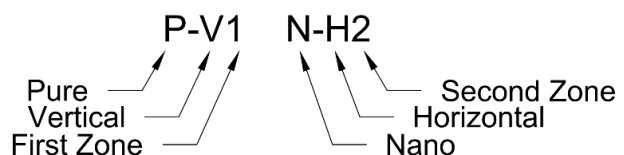


Figure 5. The notation of samples

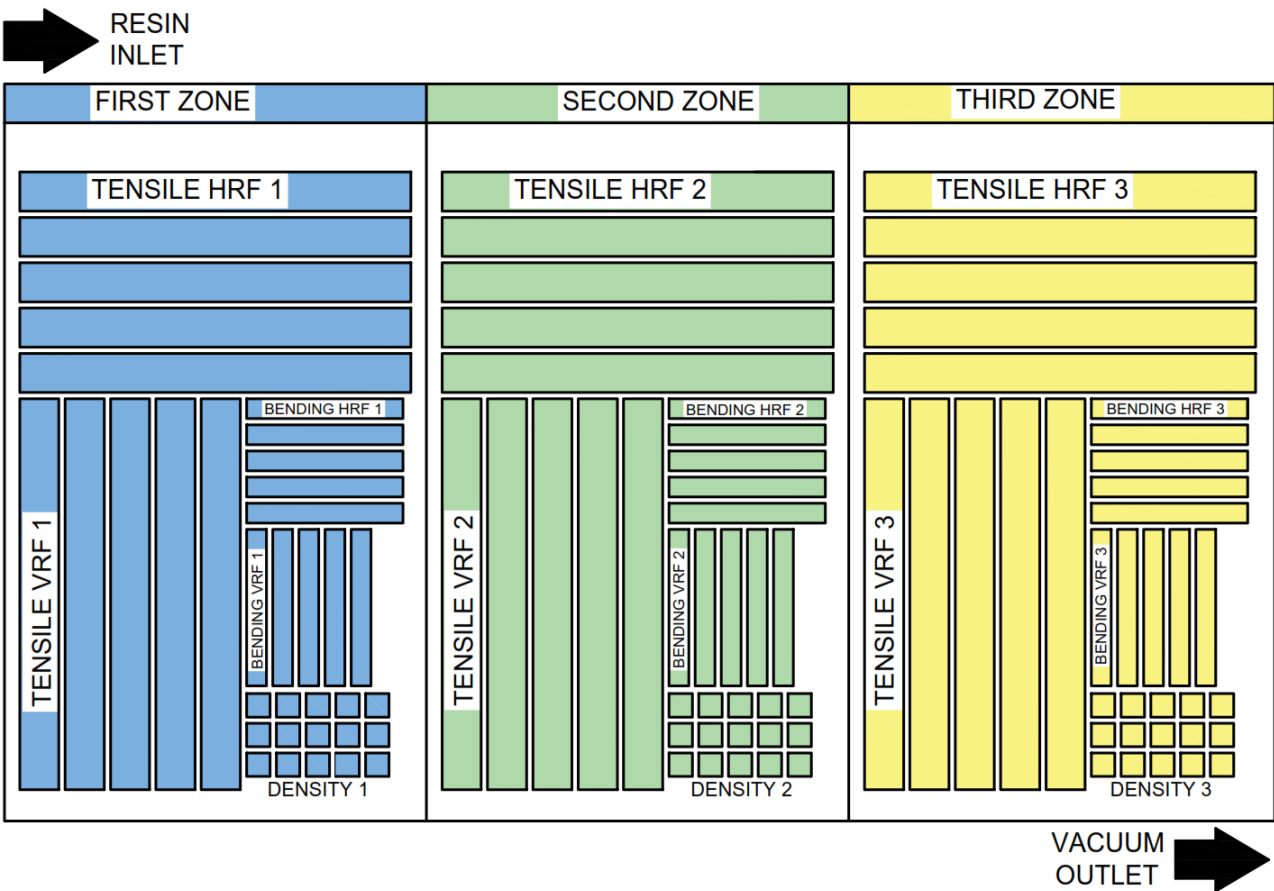


Figure 6. Sampling orientation of composite

3. Results and Discussion

3.1. Mechanical test results

Tensile, flexural and density tests were carried out using 5 samples of each parameter and the average results were taken as a basis in the graphics. Fig. 7 shows all test results. Considering the Fig. 7, it is observed that the tensile, bending and density values for both pure and nano composite increase from the 1st zone to the 3rd zone. This result is valid for both HRF and VRF samples. Normally, test results are expected to be very close to each other in pure composite. But the highest change was observed in bending.

VRF samples have an increase rate of 3.23%. This is because the resin line of the plate is long. The fact that the length of this line was around 1 m caused the compaction ratio at the vacuum side to be higher than the compaction ratio at the resin inlet. It can be concluded that the VARIM or VARTM technique was effective in compacting the fiber reinforcement under vacuum pressure,

resulting in samples with a high fiber volume percentage, consistent thickness, and minimal voids content [35]. Furthermore, the compaction pressure is restricted to the pressure of atmosphere, prohibiting the vacuum infusion process from attaining greater fiber volumetric levels [36]. Since the thickness values of the composite plate shown in Table 1 are thinner in the region where the compaction is high, stress values increase due to the cross-sectional area difference in the experimental stress calculation. Density results also confirm this phenomenon. The density values increased from the 1st zone to the 3rd zone for both composite plates. The fact that the compaction is more on the vacuum side has reduced the possible void amount, which has caused the density values to increase towards the 3rd zone.

Considering the Fig. 7-b, it is seen that the nanocomposite exhibits a similar behavior like pure one. Since the phenomena described above are also valid for this composite, all test results increased from 1st zone to the 3rd zone. However, when increase percentages in Table 2

are examined, it is seen that the increase in the test results in nanocomposite for each region is higher than in pure composite. The percentage increase rates were calculated based on how much the test results in zone 2 and 3 increased compared to zone 1. Based on the tensile test

result, an increase of 2.82% was observed in NV-3, while this rate was 1.49% in PV-3. Similarly, in bending test results, an increase of 3.31% in NV-3 and 3.23% in PV-3 was observed. Results demonstrate a consistent pattern in regions aligned horizontally with the resin flow.

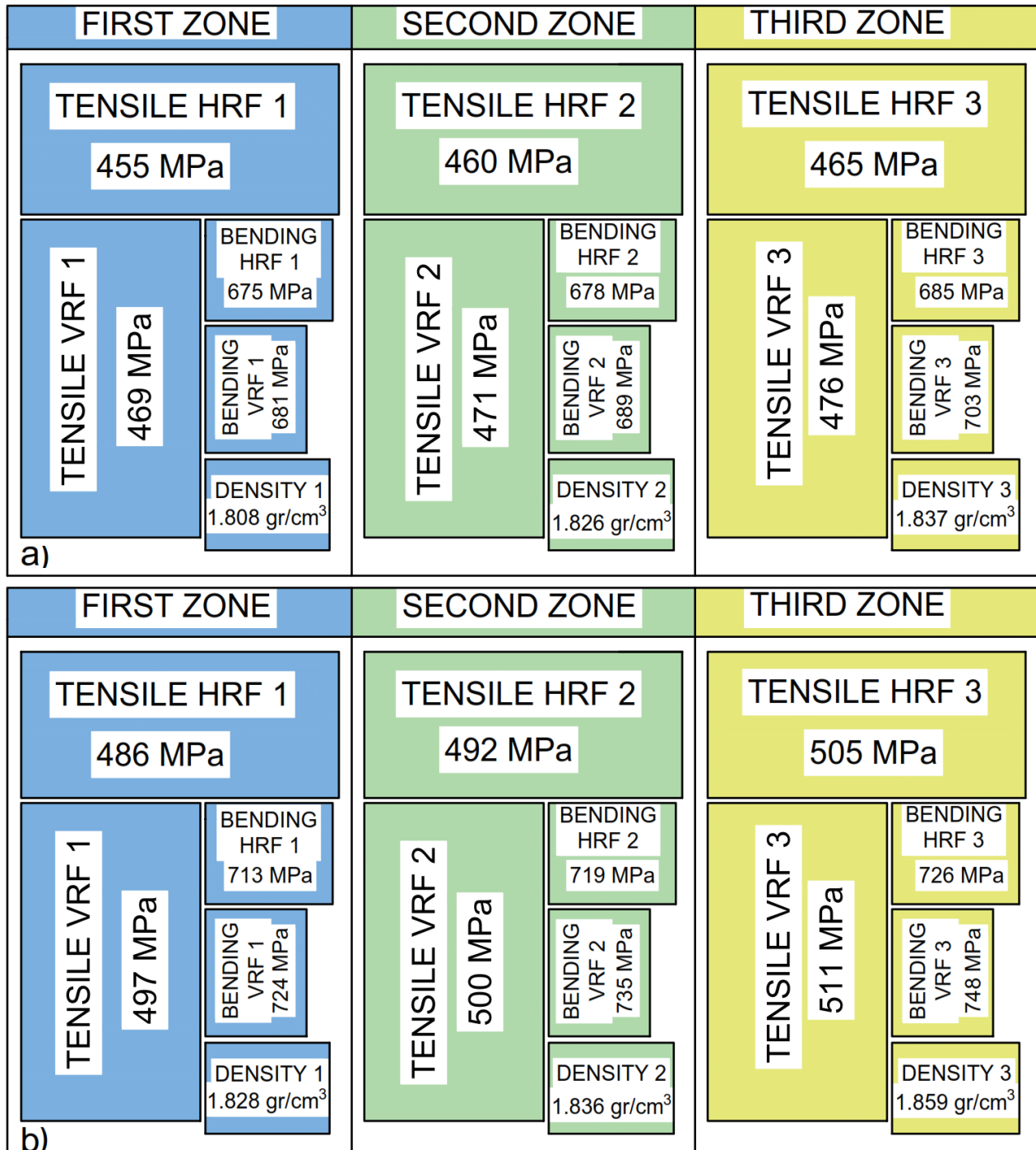


Figure 7. Test results of nanocomposite plates a) pure composite b) nanocomposite

2 wt.% of Al₂O₃ nanoparticles increased the tensile and flexural strength of glass fiber reinforced epoxy composites. Although there is variation between regions, an improvement in tensile strength from 5.97% to 8.61% was

observed. This improvement varied between 5.62% and 6.41% in flexural strength. If a comparison is made between HRF and VRF directions, it is seen that HRF values are higher than VRF values both for pure and nano

composite. This is because the thickness is more stable in the HRF direction than in the VRF direction.

Table 1. Thickness values of zones of composite plates

Zone	Thickness (mm)
Pure Zone 1	2.404
Pure Zone 2	2.374
Pure Zone 3	2.341
Nano Zone 1	2.556
Nano Zone 2	2.515
Nano Zone 3	2.476

Table 2. Percentage increase of tensile and bending test results

No.	Tensile Strength (MPa)	Perc. Increase (%)	Flexural Strength (MPa)	Perc. Increase (%)
P-V1	469±1.5	---	681±2.5	---
P-V2	471±2.6	0.43	689±3.2	1.17
P-V3	476±3.2	1.49	703±3.1	3.23
N-V1	497±1.7	---	724±2.6	---
N-V2	500±1.3	0.60	735±3.3	1.52
N-V3	511±2.4	2.82	748±2.7	3.31
P-H1	455±1.6	---	675±2.4	---
P-H2	460±1.3	1.10	678±2.8	0.44
P-H3	465±2.8	2.20	685±3.1	1.48
N-H1	486±2.2	---	713±3.2	---
N-H2	492±1.9	1.23	719±3.1	0.84
N-H3	505±2.1	3.91	726±3.4	1.82

2 wt.% of Al₂O₃ nanoparticles increased the tensile and flexural strength of glass fiber reinforced epoxy composites. Although there is variation between regions, an improvement in tensile strength from 5.97% to 8.61% was observed. This improvement varied between 5.62% and 6.41% in flexural strength. If a comparison is made between HRF and VRF directions, it is seen that HRF values are higher than VRF values both for pure and nano composite. This is because the thickness is more stable in the HRF direction than in the VRF direction. The reason why the increase between regions in nanocomposite is higher than in pure composite depends on the compaction ratio. Since compaction ratio is more on the vacuum port, the movement of the resin in the through-thickness direction is shortened in this port. Since

the nano-doped resin will travel less distance in vacuum port, the nanoparticle filtration is less in this line, resulting in relatively higher mechanical properties of the region close to the vacuum line [27]. In other words, the mechanical properties are affected by the resin flow direction. The first resin flow occurs horizontally through the infusion mesh, while the second resin flow occurs within the fiber through thickness. Hsiao et al. [37] presented an analytical solution for this and stated that a dimensionless approach with the expression given in Equation 1 is an important approach in determining the main production parameters.

$$\frac{Q_x}{Q_y} \sim \frac{K_{2xx} h_2^2}{K_{2yy} d^2} \ll 1 \quad (1)$$

The structural layer's permeabilities in the x and y directions are K_{2xx} and K_{2yy}, respectively. h₂ is the thickness of fiber preform and d is the length of flow front region.

Tensile and flexural test results were also given as stress-strain graphics in Fig.8 and Fig.9, respectively. Tensile and bending forces represent fundamental aspects of mechanical loading, constituting two of the five primary types of loads in the field. The stress-strain curves of fiber-reinforced polymer composites under tensile and bending forces are different from each other. Since FRP composites are in a brittle structure, they do not have yield points [38]. When the tensile stress-strain curves (Fig.8) are examined, the curves demonstrate a linear relationship and the sample is suddenly broken without any yielding. The rupture happens without any obvious difference in the rate of elongation [39]. The curves obtained in this study are similar to the typical curves observed in FRP composites. No abnormality was found between the curves of pure and nanocomposite or between the curves of VRF and HRF zones. A similar trend occurred in bending (flexural) curves. But here, when the stress reaches its maximum point, the fracture does not occur suddenly, as in tensile test. Once stress reaches its peak, the sample sustains bending load until a specific threshold, as bending stress is highest at the specimen's surface and zero at the neutral axis. This behavior reflects the material's capacity to withstand bending forces and highlights the distribution of

stress across the specimen. The normal bending stress changes linearly according to the distance from the neutral axis in the elastic range. Therefore, the surface of the sample is subjected to maximum stress and the fibers on the surface begin to rupture first. The rupture of fibers continues gradually from the surface to the neutral axis. This means that the fracture event

occurs with a long strain and this causes the flexural stress-strain curves to form as in Fig. 9. Fig. 10 shows the damage mechanism of tested samples. The reason for the behavior of flexural stress-strain curves is more clearly understood with this figure. The fiber ruptures on the surface of the sample are clearly visible.

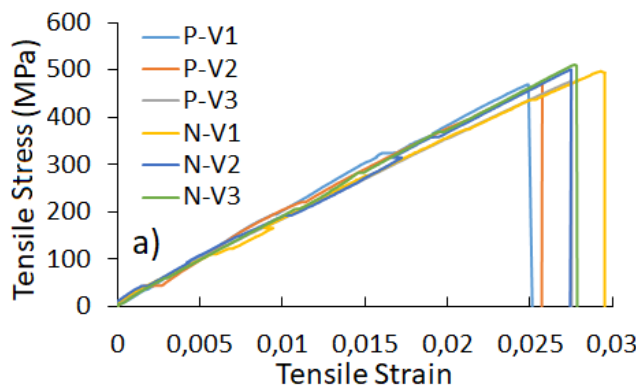


Figure 8. Tensile strength-strain curves of composite plates a) vertical to the resin flow (VRF) b) horizontal to the resin flow (HRF)

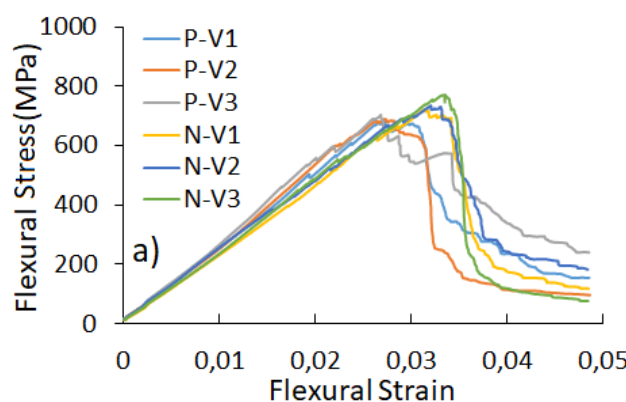
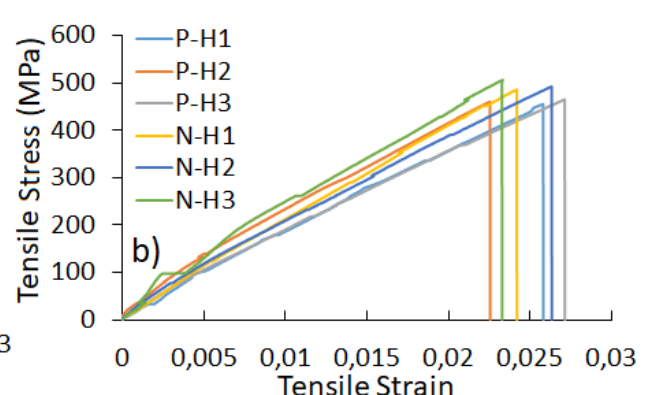
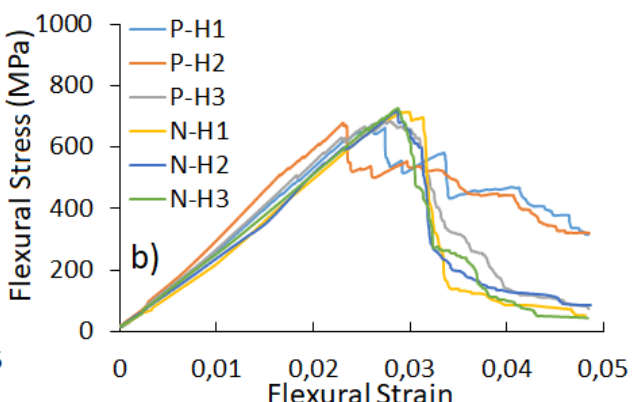


Figure 9. Flexural strength-strain curves of composite plates a) vertical to the resin flow (VRF) b) horizontal to the resin flow (HRF)



In tensile test samples, failure modes should be analyzed according to ASTM D3039 standard. In this standard three-character coding is used to identify failure modes. The first character represents the failure type, the second character represents the failure area, and the third character represents the failure location. The failure types with respect to coding system were shown in Fig. 10. The first character "L" represents the lateral failure type observed similarly in all samples. The second character "M" and "A" are the failure area codes of "multiple areas" and "at grip", respectively. These two failure areas were observed predominantly in all samples. The third character, "V" and "T" are failure location codes of "various" and "top", respectively. These two

failure locations are valid for all samples. Damage mechanisms with the above codes were observed in all samples regardless of nanoparticle contribution and sampling orientation.

The first character "L" represents the lateral failure type observed similarly in all samples. The second character "M" and "A" are the failure area codes of "multiple areas" and "at grip", respectively. These two failure areas were observed predominantly in all samples. The third character, "V" and "T" are failure location codes of "various" and "top", respectively. These two failure locations are valid for all samples. Damage mechanisms with the above codes were

observed in all samples regardless of nanoparticle contribution and sampling orientation. The SEM images of nanocomposite tensile test samples are shown in Fig.11. The homogeneous distribution of nanoparticles is shown in the surface image in Figure 11-a. The

various damage modes, encompassing fiber fracture, matrix breakage, and delamination are demonstrated in Fig. 11b and Fig. 11c. It can be seen in Fig.11b that nano Al_2O_3 particles strengthen the matrix-fiber bonding



Figure 10. Damage mechanism of tensile and flexural test samples

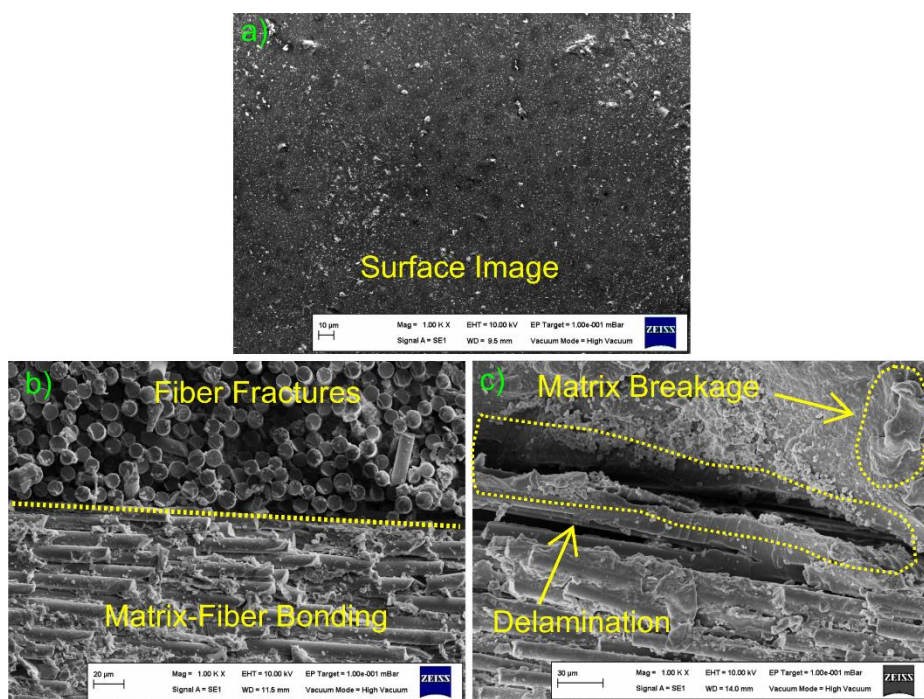


Figure 11. SEM images of test sample

3.2. Statistical analysis (ANOVA)

One-way ANOVA analysis was used to determine whether the means of three independent variables were statistically significant [40]. The three different variables are the first, second and third zones from which the samples are extracted. A null hypothesis (H_0) is needed to use the ANOVA test. In this study, the H_0 hypothesis was considered as “there is no difference between the means for three different regions.” To test this hypothesis, strength values was used as dependent variable and three different regions were used as factor variables. First, to test the hypothesis, the data of the PV samples were tested using the IBM SPSS Statistics 22. Table 3 shows the descriptives of PV samples for tensile strength. N represents the number of samples and tests were performed at the 95% Confidence Interval for the Mean.

After determining the descriptives, the one-way ANOVA analysis was performed. Table 4 shows

the results of PV samples for tensile strength. df means degree of freedom and F is the variance of the group means. The value in the last column indicates statistical significance. It's generally represented by P-Value. The null hypothesis should be assessed by comparing the P-value to the significance level to see if any of the comparison of means are statistically significant. A significance score of 0.05 is usually sufficient. With a significance level of 0.05, there's a 5% chance of determining that a difference exists. The null hypothesis is rejected if the P-value is below or equal to the significance level [41]. If the P-value is greater, the null hypothesis is accepted. In Table 4, the P-value is 0.104, which is greater than 0.05 and the hypothesis is accepted. It means that there is no difference between the means for three different regions. Although the experimental results show an increase from the first zone to the third zone for PV samples, statistical analysis indicates that this change is not significant.

Table 3. Descriptives of PV (Pure-Vertical) samples

N	Mean	Std.		95% Confidence		Interval for Mean	
		Deviation	Error	Lower Bound	Upper Bound	Minimum	Maximum
PV-1	5	469.4306	5.15650	2.30606	463.0280	475.8332	463.33 475.41
PV-2	5	471.1172	4.96969	2.22251	464.9465	477.2879	465.77 476.62
PV-3	5	476.0494	3.63552	1.62585	471.5353	480.5635	470.47 480.50
Total	15	472.1991	5.18457	1.33865	469.3279	475.0702	463.33 480.50

Table 4. One way ANOVA of PV (Pure-Vertical) samples

	Sum of Squares		Mean Square		
	df	F	P		
Between Groups	118.300	2	59.150	2.751	0.104
Within Groups	258.017	12	21.501		
Total	376.316	14			

Normally, if the null hypothesis is accepted, the analysis is not continued. Because the result already indicates that the mean of the independent variables is not significant. However, Tukey test from post hoc analysis is

given in Table 5 to show that the results between groups are not significant. Tensile stress variables of PV-1, PV-2 and PV-3 samples were evaluated among themselves and P-values were higher than 0.05 in all comparisons. This means that although there is an experimental difference between the stress values of the tensile samples extracted from three different zones, this difference is not statistically significant. The above-mentioned analysis was performed for only one parameter. Since it is meaningless to give each table in detail for each parameter, the results of ANOVA analysis, which is the most important table for all parameters, are given in Table 6. All p-values for each parameter are greater than 0.05. This shows that in all samples, from the first region to the third region, the test

results are not statistically significant in terms of tensile and flexural stress for both pure and nanocomposite. The fact that group comparisons do not show a statistically significant difference does not mean that the experimental results are insignificant. According to McLean and Ernest [42], significance tests may not give information regarding the practical importance of an event or whether the result can be replicated. Slight differences between experimental results make sense in the test evaluation. In the realm of experimental applications, it is of paramount

importance to meticulously extract the samples from precisely the same orientation. This meticulous approach ensures that the samples being compared are not only consistent but also align perfectly, thereby enhancing the accuracy and reliability of the results obtained. This critical step serves as the cornerstone for the entire experimental process, laying the foundation for meaningful and robust evaluations that can lead to invaluable insights and scientific advancements.

Table 5. Multiple comparisons (Tukey) of PV (Pure-Vertical) samples

			95% Confidence Interval			
Groups (I)	Groups (J)	(I-J)	Mean Difference	Std.	Lower	Upper
			Error	P	Bound	Bound
PV-1	PV-2	-1.68660	2.93267	.836	-9.5106	6.1374
	PV-3	-6.61880	2.93267	.101	-14.4428	1.2052
PV-2	PV-1	1.68660	2.93267	.836	-6.1374	9.5106
	PV-3	-4.93220	2.93267	.252	-12.7562	2.8918
PV-3	PV-1	6.61880	2.93267	.101	-1.2052	14.4428
	PV-2	4.93220	2.93267	.252	-2.8918	12.7562

Table 6. One-way ANOVA test results of all parameters

Groups	Types	Sum of Squares	df	Mean Square	F	P
PV (Tensile)	Between Groups	118.300	2	59.150	2.751	.104
PH (Tensile)	Between Groups	248.914	2	124.457	1.986	.180
NV (Tensile)	Between Groups	521.307	2	260.654	3.041	.085
NH (Tensile)	Between Groups	970.601	2	485.301	2.344	.138
PV (Flexural)	Between Groups	1199.749	2	599.874	1.190	.338
PH (Flexural)	Between Groups	267.103	2	133.551	.540	.597
NV (Flexural)	Between Groups	1430.553	2	715.276	.366	.432
NH (Flexural)	Between Groups	482.234	2	241.117	1.038	.384

4. Conclusion

The VARTM or VARIM method employed in the production of nanocomposites is a subject that demands examination from various perspectives, particularly concerning nanoparticle filtration. In this study, two types of materials were manufactured: pure glass fiber-reinforced composites and glass fiber-reinforced nanocomposites with a 2 wt.% Al₂O₃ doping. The study investigated the effects of extracting samples from different zones and orientations within both the pure and nanocomposite materials. Samples were collected from three

distinct zones: the resin inlet zone (First), the middle zone (Second), and the vacuum outlet zone (Third). Additionally, two directions were considered: horizontal to the resin flow (HRF) and vertical to the resin flow (VRF) to provide a comprehensive assessment of the mechanical properties of the composites. Mechanical property assessments were conducted, including tensile, three-point bending, and density tests. As a result, there was a notable increase in tensile, bending, and density values when moving from the first zone to the third zone in both pure and nanocomposites. This increase can be attributed to the slightly higher pressure at the

vacuum outlet compared to the pressure at the resin inlet. It is worth noting that the plates used in this study had a length of approximately 1 meter. The pressure differential led to variations in thickness, resulting in stress value differences of up to 3.91%, with the nanocomposites exhibiting more pronounced variations compared to the pure composites.

The reduction in nanoparticle filtration through-thickness in the vacuum outlet region can be explained by the thinner thickness of the vacuum outlet compared to the resin inlet due to compaction. This shorter travel distance for the nano-doped resin in the vacuum outlet resulted in enhanced mechanical properties in the vicinity of the vacuum outlet, as supported by the density measurements. Notably, the density values of both composite plates increased from the first to the third zone due to reduced potential voids caused by higher compaction on the vacuum side. In the context of nanocomposite production, using smaller-sized plates has proven to yield more consistent outcomes. It's also important to mention that the horizontal to the resin flow (HRF) values consistently exceeded the vertical to the resin flow (VRF) values, highlighting the greater thickness stability in the HRF direction. To ensure accurate comparisons between stress values of samples across different plates, it is essential to extract samples with the same orientation and from the same zone.

To assess the statistical significance of the means of three independent variables, a one-way ANOVA analysis was conducted. The null hypothesis (H_0) posited that there was no difference in means across three different regions. The null hypothesis was accepted, as the calculated p-value of 0.104 exceeded the significance level of 0.05. This result indicates that there is no statistically significant difference in means among the three distinct regions.

While experimental observations may suggest an increase in test results from the first to the third zones, the statistical analysis reveals that this shift is not significant. However, it's important to note that a lack of statistical significance does not render experimental results meaningless. Instead, it indicates the absence of a clear correlation. Nonetheless, for a more precise interpretation of

the results, it remains crucial to consistently extract samples from the same zone and orientation in experimental tests.

Article Information Form

Funding

The author has not received any financial support for the research, authorship, or publication of this study.

Authors' Contribution

The author confirms sole responsibility for the following: study conception and design, data collection, analysis and interpretation of results, and manuscript preparation.

The Declaration of Conflict of Interest/

Common Interest

The author declares that they have no known competing financial interests or personal relationships that could have appeared to influence the work reported in this paper.

The Declaration of Ethics Committee Approval

This study does not require ethics committee permission or any special permission.

The Declaration of Research and Publication Ethics

The author of the paper declares that he complies with the scientific, ethical, and quotation rules of SAUJS in all processes of the paper and that they do not make any falsification on the data collected. In addition, he declares that Sakarya University Journal of Science and its editorial board have no responsibility for any ethical violations that may be encountered and that this study has not been evaluated in any academic publication environment other than Sakarya University Journal of Science.

Copyright Statement

The author owns the copyright of their work published in the journal and their work is published under the CC BY-NC 4.0 license

References

- [1] G. Demircan, M. Kisa, M. Ozen, A. Acikgoz, Y. Işiker, E. Aytar, "Nanogelcoat application of glass fiber reinforced

- polymer composites for marine application: Structural, mechanical, and thermal analysis," *Marine Pollution Bulletin*, vol. 194, p. 115412, 2023.
- [2] T. Singh, B. Gangil, L. Ranakoti, A. Joshi, "Effect of silica nanoparticles on physical, mechanical, and wear properties of natural fiber reinforced polymer composites," *Polymer Composites*, vol. 42, no. 5, pp. 2396–2407, 2021.
- [3] G. Demircan, M. Ozen, M. Kisa, A. Acikgoz, Y. Işiker, "The effect of nano-gelcoat on freeze-thaw resistance of glass fiber-reinforced polymer composite for marine applications," *Ocean Engineering*, vol. 269, p. 113589, 2023.
- [4] K. Srinivasan, W. C. Jackson, B. T. Smith, J. A. Hinkley, "Characterization of damage modes in impacted thermoset and thermoplastic composites," *Journal of Reinforced Plastics and Composites*, vol. 11, no. 10, pp. 1111–1126, 1992.
- [5] G. Demircan, M. Kisa, M. Ozen, A. Acikgoz, "Quasi-Static Penetration behavior of glass-fiber-reinforced epoxy nanocomposites," *Mechanics of Composite Materials*, vol. 57, no. 4, pp. 503–516, Sep. 2021.
- [6] A. Siddika, M. A. Al Mamun, R. Alyousef, Y. H. M. Amran, "Strengthening of reinforced concrete beams by using fiber-reinforced polymer composites: A review," *Journal of Building Engineering*, vol. 25, p. 100798, 2019.
- [7] J. J. Kenned, K. Sankaranarayanasamy, J. S. Binoj, S. K. Chelliah, "Thermo-mechanical and morphological characterization of needle punched non-woven banana fiber reinforced polymer composites," *Composites Science and Technology*, vol. 185, p. 107890, 2020.
- [8] M. Özen, G. Demircan, M. Kisa, Z. Ilik, "Investigation of usability of waste textile fabrics in composites," *Emerging Materials Research*, vol. 9, no. 1, pp. 1–6, Mar. 2020.
- [9] T. D. Tavares, J. C. Antunes, F. Ferreira, H. P. Felgueiras, "Biofunctionalization of natural fiber-reinforced biocomposites for biomedical applications," *Biomolecules*, vol. 10, no. 1, p. 148, Jan. 2020.
- [10] Y. Li, N. Li, J. Gao, "Tooling design and microwave curing technologies for the manufacturing of fiber-reinforced polymer composites in aerospace applications," *The International Journal of Advanced Manufacturing Technology*, vol. 70, no. 1–4, pp. 591–606, 2013.
- [11] D. K. Rajak, D. D. Pagar, P. L. Menezes, E. Linul, "Fiber-reinforced polymer composites: Manufacturing, properties, and applications," *Polymers (Basel)*, vol. 11, no. 10, p. 1667, Oct. 2019.
- [12] A. T. Bhatt, P. P. Gohil, V. Chaudhary, "Primary manufacturing processes for fiber reinforced composites: History, development & future research trends," *IOP Conference Series: Materials Science and Engineering*, vol. 330, p. 12107, 2018.
- [13] J. P. Davim, P. Reis, C. C. António, "Experimental study of drilling glass fiber reinforced plastics (GFRP) manufactured by hand lay-up," *Composites Science and Technology*, vol. 64, no. 2, pp. 289–297, 2004.
- [14] S. G. Advani C. L. Tucker, "A numerical simulation of short fiber orientation in compression molding," *Polymer Composites*, vol. 11, no. 3, pp. 164–173, 1990.
- [15] N. O. Cabrera, B. Alcock, E. T. J. Klompen, T. Peijs, "Filament winding of

- co-extruded polypropylene tapes for fully recyclable all-polypropylene composite products," *Applied Composite Materials*, vol. 15, no. 1, pp. 27–45, 2008.
- [16] X. Peng, M. Fan, J. Hartley, M. Al-Zubaidy, "Properties of natural fiber composites made by pultrusion process," *Journal of Composite Materials*, vol. 46, no. 2, pp. 237–246, 2011.
- [17] J. H. Jeon, C. K. Yoon, S. H. Park, W. Il Lee, S. M. Kim, "Assessment of long fiber spray-up molding of chopped glass fiber reinforced polydicyclopentadiene composites," *Fibers and Polymers*, vol. 21, no. 5, pp. 1134–1141, 2020.
- [18] M. A. Agwa, S. M. Youssef, S. S. Ali-Eldin, M. Megahed, "Integrated vacuum assisted resin infusion and resin transfer molding technique for manufacturing of nano-filled glass fiber reinforced epoxy composite," *Journal of Industrial Textiles*, vol. 51, no. 3_suppl, pp. 5113S-5144S, 2020.
- [19] M. Ozen, G. Demircan, M. Kisa, A. Acikgoz, G. Ceyhan, Y. Isiker, "Thermal properties of surface-modified nano-Al₂O₃/Kevlar fiber/epoxy composites," *Mater. Materials Chemistry and Physics*, vol. 278, p. 125689, Feb. 2022.
- [20] U. K. Vaidya, M. V Kamath, H. Mahfuz, S. Jeelani, "Low velocity impact response of Resin Infusion Molded foam filled honeycomb sandwich composites," *Journal of Reinforced Plastics and Composites*, vol. 17, no. 9, pp. 819–849, 1998.
- [21] G. Demircan, M. Kisa, M. Özen, A. Açıkgöz, B. Aktaş, M. Ali Kurt, "A bio-based epoxy resin from rosin powder with improved mechanical performance," *Emerging Materials Research*, vol. 9, no. 4, pp. 1076–1081, Dec. 2020.
- [22] M. Sánchez, M. Campo, A. Jiménez-Suárez, A. Ureña, "Effect of the carbon nanotube functionalization on flexural properties of multiscale carbon fiber/epoxy composites manufactured by VARIM," *Composites Part B: Engineering*, vol. 45, no. 1, pp. 1613–1619, 2013.
- [23] Z. A. Oguz, A. Erklig, Ö. Y. Bozkurt, "Degradation of hybrid aramid/glass/epoxy composites hydrothermally aged in distilled water," *Journal of Composite Materials*, vol. 55, no. 15, pp. 2043–2060, 2020.
- [24] A. Hindersmann, "Confusion about infusion: An overview of infusion processes," *Composites Part A: Applied Science and Manufacturing*, vol. 126, p. 105583, 2019.
- [25] R. Matsuzaki, S. Kobayashi, A. Todoroki, Y. Mizutani, "Full-field monitoring of resin flow using an area-sensor array in a VaRTM process," *Composites Part A: Applied Science and Manufacturing*, vol. 42, no. 5, pp. 550–559, 2011.
- [26] G. Demircan, M. Kisa, M. Ozen, B. Aktas, "Surface-modified alumina nanoparticles-filled aramid fiber-reinforced epoxy nanocomposites: preparation and mechanical properties," *Iranian Polymer Journal*, vol. 29, no. 3, pp. 253–264, Mar. 2020.
- [27] M. Özer, H. Ulus, H. B. Kaybal, "Enhanced out-of-plane loading performance of multi-scale glass/epoxy composites doped with HNTs," *International Journal of Pioneering Technology and Engineering*, vol. 2 no. 01, pp. 99-102, 2023.
- [28] H. Ulus, "The impact of seawater aging on basalt/graphene nanoplatelet-epoxy composites: performance evaluating by Dynamic Mechanical Analysis (DMA) and

- short beam shear (sbs) tests” Niğde Ömer Halisdemir Üniversitesi Mühendislik Bilimleri Dergisi, vol.10 no.1, pp. 412-419, 2021.
- [29] K.-T. Hsiao D. Heider, “Vacuum assisted resin transfer molding (VARTM) in polymer matrix composites,” Manufacturing Techniques for Polymer Matrix Composites (PMCs). Elsevier, pp. 310–347, 2012.
- [30] Z. Fan, M. H. Santare, S. G. Advani, “Interlaminar shear strength of glass fiber reinforced epoxy composites enhanced with multi-walled carbon nanotubes,” Composites Part A: Applied Science and Manufacturing, vol. 39, no. 3, pp. 540–554, 2008.
- [31] S. Movva, G. Zhou, D. Guerra, L. J. Lee, “Effect of carbon nanofibers on mold filling in a vacuum assisted Resin Transfer Molding system,” Journal of Composite Materials, vol. 43, no. 6, pp. 611–620, 2009.
- [32] H. B. Kaybal, H. Ulus, O. Demir, Ö. S. Şahin, A. Avci, “Effects of alumina nanoparticles on dynamic impact responses of carbon fiber reinforced epoxy matrix nanocomposites,” Engineering Science and Technology, an International Journal, vol. 21 no.3, pp. 399-407, 2018.
- [33] “Test Method for Tensile Properties of Polymer Matrix Composite Materials.” ASTM International. ASTM D3039/D3039M-17, West Conshohocken, PA, 2017.
- [34] “Test Methods for Flexural Properties of Unreinforced and Reinforced Plastics and Electrical Insulating Materials.” ASTM International. ASTM D790-17, West Conshohocken, PA, 2017.
- [35] U. R. Hashim, A. Jumahat, M. Jawaid, “Mechanical properties of hybrid graphene nanoplatelet-nanosilica filled unidirectional basalt fibre composites,” Nanomaterials (Basel, Switzerland), vol. 11, no. 6, p. 1468, Jun. 2021.
- [36] G. Francucci, S. Palmer, W. Hall, “External compaction pressure over vacuum-bagged composite parts: Effect on the quality of flax fiber/epoxy laminates,” Journal of Composite Materials, vol. 52, no. 1, pp. 3–15, 2017.
- [37] K.-T. Hsiao, R. Mathur, S. G. Advani, Gillespie J. W., B. K. Fink, “A closed form solution for flow during the vacuum assisted Resin Transfer Molding Process,” Journal of Manufacturing Science and Engineering, vol. 122, no. 3, pp. 463–475, 1999.
- [38] S. Cao, Z. Wu, X. Wang, “Tensile Properties of CFRP Hybrid FRP Composites at Elevated Temperatures,” Journal of Composite Materials, vol. 43, no. 4, pp. 315–330, 2009.
- [39] A. C. N. Singleton, C. A. Baillie, P. W. R. Beaumont, T. Peijs, “On the mechanical properties, deformation and fracture of a natural fibre/recycled polymer composite,” Composites Part B: Engineering, vol. 34, no. 6, pp. 519–526, 2003.
- [40] R. M. Heiberger E. Neuwirth, “One-Way ANOVA,” R Through Excel. Springer New York, pp. 165–191, 2009.
- [41] J. P. Verma, “One-Way ANOVA: Comparing Means of More than Two Samples,” Data Analysis in Management with SPSS Software. Springer India, pp. 221–254, 2012.
- [42] J. E. McLean, J. M. Ernest, “The role of statistical significance testing in educational research,” Research in the Schools, vol. 5 no. 2, 1998.